

# Radiation measurement in the environment of FLASH using passive dosimeters

B Mukherjee<sup>1</sup>, D Rybka<sup>2,3</sup>, D Makowski<sup>4</sup>, T Lipka<sup>5</sup>  
and S Simrock<sup>1</sup>

<sup>1</sup> Deutsches Elektronen-Synchrotron (DESY), Accelerator Radiation Control Group (MSK), Notkestrasse 85, D-22607 Hamburg, Germany

<sup>2</sup> Institute of Electronic Systems, Warsaw University of Technology, Ul. Nowowiejska 15/19, 00-665 Warszawa, Poland

<sup>3</sup> The Andrzej Sołtan Institute of Nuclear Studies, 05-400 Świerk/Otwock, Poland

<sup>4</sup> Department of Microelectronics and Computer Science, Technical University of Lodz, Al. Politechniki 11, 90-924 Lodz, Poland

<sup>5</sup> Institute for Measurement Technology, Technical University Hamburg Harburg, Harburger Schloßstrasse 20, D-21079 Hamburg, Germany

E-mail: [mukherjee@ieee.org](mailto:mukherjee@ieee.org)

Received 16 November 2006, in final form 19 February 2007

Published 6 July 2007

Online at [stacks.iop.org/MST/18/2387](http://stacks.iop.org/MST/18/2387)

## Abstract

Sophisticated electronic devices comprising sensitive microelectronic components have been installed in the close proximity of the 720 MeV superconducting electron linear accelerator (linac) driving the FLASH (Free Electron Laser in Hamburg), presently in operation at DESY in Hamburg. Microelectronic chips are inherently vulnerable to ionizing radiation, usually generated during routine operation of high-energy particle accelerator facilities like the FLASH. Hence, in order to assess the radiation effect on microelectronic chips and to develop suitable mitigation strategy, it becomes imperative to characterize the radiation field in the FLASH environment. We have evaluated the neutron and gamma energy (spectra) and dose distributions at critical locations in the FLASH tunnel using superheated emulsion (bubble) detectors, GaAs light emitting diodes (LED), LiF-thermoluminescence dosimeters (TLD) and radiochromic (Gafchromic EBT) films. This paper highlights the application of passive dosimeters for an accurate analysis of the radiation field produced by high-energy electron linear accelerators.

**Keywords:** bremsstrahlung, electron linear accelerator, free electron laser, passive radiation dosimeters, photoneutrons, radiation dosimetry, radiation effect, superconducting cavities, XFEL

## 1. Introduction

In April 2006, at DESY the free electron laser FLASH (Free Electron Laser in Hamburg), generating very high brilliance vacuum-ultraviolet ( $\lambda = 13$  nm) light started routine operation. The FLASH is driven by a 720 MeV (upgradeable to 1 GeV) superconducting electron linac based on ultra pure niobium cavities, developed on TESLA technology. Furthermore, the

FLASH will serve as the prototype of the much larger and more powerful European X-Ray Free Electron Laser (XFEL), already under construction in Hamburg [1].

Advanced measurement and control instruments based on state-of-the-art microelectronics have been mounted inside the FLASH containment tunnel, in most cases quite close to the electron linac. Evidently, during the operation of FLASH those electronic devices are subjected to a stray

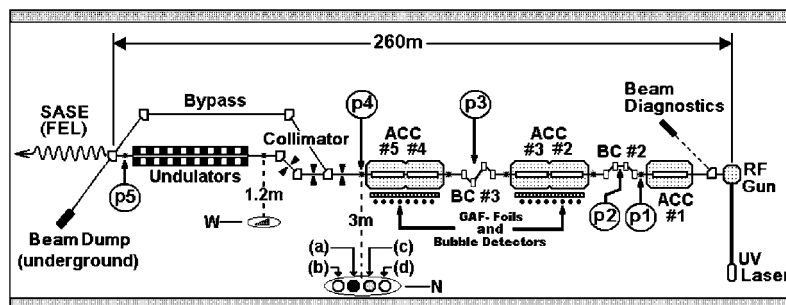


**Figure 1.** Showing the main components of the FLASH facility; p1, p2, p3 and p4 are the locations where radiation measurements were made using GaAs LED. The figure is explained in detail in the main text.

radiation field produced by the linac, thereby enhancing the risk of radiation-induced malfunction of the above devices. A flawless performance of the electronic instrumentation systems is mandatory to safe and uninterrupted operation of the FLASH [2]. Hence, it becomes imperative to monitor the radiation effect on electronics installed in the FLASH radiation environment on both a long- and short-term basis.

Conventional radiation monitoring devices are usually bulky and the associated nuclear electronics is susceptible to pulse-pile-up and dead time effects [3]. These pitfalls make them unsuitable for radiation detection at FLASH, since the electron linac driving the FLASH operates at a repetition rate of 10 Hz. Furthermore, one often has to assess radiation doses at ‘difficult to reach’ locations (niches) along the linac. To circumvent the above shortcomings we have developed novel passive dosimetry techniques based on commercial off-the-shelf (COTS) gallium arsenide (GaAs) light emitting diodes (LED) [4], superheated emulsion (bubble) detectors (types: BDPND and BDT; manufacturer: Bubble Technology Industries, Chalk River, Canada) [5], thermoluminescent dosimeters (TLD) [6] and radiochromic films (type: Gafchromic, Gaf-EBT; manufacturer: International Specialty Product, NJ, USA) [7]. This paper highlights the experimental methods and the results of neutron and gamma dosimetry/spectrometry performed with various types of passive dosimeters in the FLASH environment.

### 1.1. Operation principle of the linac driving the FLASH

The schematic diagram of the superconducting electron linac driving the FLASH highlighting the locations of radiation measurement using various passive dosimeters is shown in figure 1.

At FLASH the high quantum efficiency photo-cathode ( $\text{Cs}_2\text{Te}$ ) of the RF gun is excited by a pulsed ( $f = 1.3$  GHz) UV ( $\lambda = 260$  nm) laser beam facilitating photoemission of electrons [8]. These photoelectrons are accelerated to 4 MeV in the RF gun which also includes a  $1\frac{1}{2}$  cell cavity, the initial electron beam is injected into accelerator module 1 (ACC #1), accelerated to 150 MeV, and subsequently delivered to the accelerator modules 2 and 3 (ACC #2/ACC #3) via bunch compressor BC #2, thereby boosting the electron beam energy to 450 MeV. In the final stage, the energetic electron beam is fed to accelerator modules 4 and 5 (ACC #4/ACC #5) through

bunch compressor BC #3, attaining a maximum energy of 720 MeV.

The accelerated electron beam is collimated and guided through a 27 m long undulator, made of an array of tiny permanent magnet pellets to produce a self-amplified spontaneous emission free electron laser (SASE FEL) beam [9]. Finally, the accelerated electron beam is stopped in a water-cooled, underground beam dump. Furthermore, a bypass beam-pipe located above the undulator array facilitates the research and development applications of the high-energy electron beam without hampering the undulator operation.

The electron beam passes through bunch compressors BC #2 and BC #3 after being accelerated via modules ACC #1 and ACC #3, respectively. In the bunch compressors, the electron beam follows a zigzag path through the ‘magnetic chicane’ resulting in longitudinal compression, bringing the initial electron bunch length of about 1 mm down to about  $250\ \mu\text{m}$  [10]. On the other hand, in the collimator the electron beam traverses a bowed ‘dog leg’ path and is narrowed to a cross section of a few micrometres diameter. The aim of the collimator is to prevent the collision of the electron beam with the undulator, thereby protecting magnet pellets from radiation damage [1]. In the bunch compressors as well as the collimator, a significant number of transversally emitted electrons hit the internal wall of the beam pipe producing a high radiation background.

### 1.2. Radiation produced by field emission electrons in the cavity

The high gradient ( $\sim 25$  MV  $\text{m}^{-1}$ ) applied across the superconducting, high purity niobium cavities of the accelerator modules driving the FLASH causes a significant level of field emission electrons [11]. These field emission electrons are accelerated within the accelerator modules, hitting the internal wall surface resulting in the production of a strong radiation field predominantly made of gamma rays (bremsstrahlung) and photoneutrons. The field emission is a quantum-mechanical phenomenon (tunnel effect) described by the well-known Fowler Nordheim equation [12] as shown below:

$$J_{\text{FN}} = \left(\frac{C}{\phi}\right) (\beta E)^2 \exp\left(-\frac{B\phi^{3/2}}{\beta E}\right) \quad (1)$$

where  $J_{\text{FN}}$  stands for the field emission current density ( $\text{A cm}^{-2}$ ),  $\phi$  is the work function (eV) of the surface

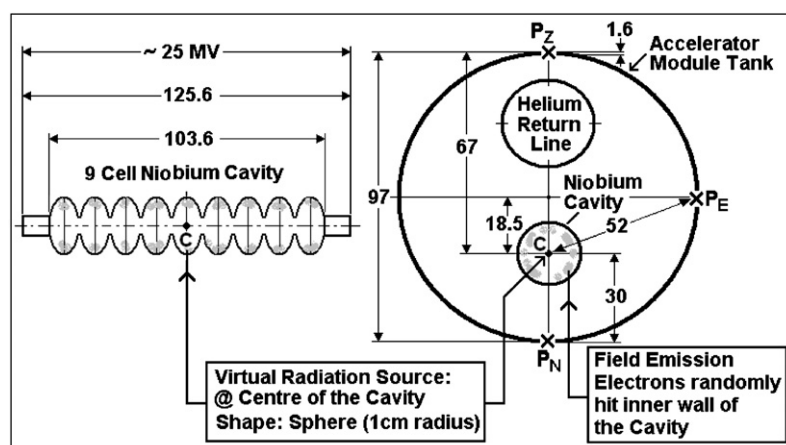


**Figure 2.** Showing the important dimensions (in centimetres) of the accelerator module tank and nine-cell niobium cavity developed on TESLA technology at DESY.

**Table 1.** Important mechanical and physical parameters of the superconducting niobium cavity developed on TESLA technology at DESY [13].

Parameter	Type/value
Acceleration type	Standing wave
Acceleration mode	$2\pi$
Fundamental frequency	1.3 GHz
Cavity gradient	$25 \text{ MV m}^{-1}$ (routine operation)
Quality factor (QF)	$> 5 \times 10^9$
Active length	103.6 cm
Number of cells	9
Cell-to-cell coupling	1.87 %
Work function (Nb)	4.3 eV
Iris diameter	7 cm
RF pulse duration	$1330 \mu\text{s}$
Repetition rate	10 Hz (routine operation)
Filling time	$530 \mu\text{s}$
Beam acceleration time (flat top)	$800 \mu\text{s}$
RF power: peak/average	208 kW/1.4 kW
Number of HOM couplers	2
Number of power couplers	1
Liquid helium temperature	2 K

material (niobium),  $\beta$  is the geometrical factor due to surface irregularity effect and  $E$  is the electric field strength (gradient) ( $\text{V m}^{-1}$ ). Furthermore,  $B$  ( $\text{V m}^{-1}$ ) and  $C$  ( $\text{A V}^{-1}$ ) are material specific constants. Equation (1) implies an exponential growth of the field emission current density with the electric field gradient across the cavity.

The schematic diagram elucidating the principle of field emission in the nine-cell superconducting niobium cavities used in the accelerator modules described in this paper is shown in figure 2. The basic structural details, including the dimensions of the nine cell superconducting niobium cavity [13], are shown on the left-hand side of figure 2. The configuration and the dimensions of the accelerator module tank (made of 16 mm thick steel) and the positions of the cavity and helium return line are shown on the right-hand side. The spots  $P_N$ ,  $P_E$ ,  $P_Z$  and  $C$  indicate the locations of passive dosimeters, used for *in situ* dosimetry of radiation emanated from the cavity and the virtual radiation source (kernel), respectively. Important design parameters of the superconducting TESLA cavity are summarized in table 1.

## 2. Materials and methods

### 2.1. The type and purpose of radiation dosimeters deployed

Within the framework of the present research project, we have exclusively used passive radiation detectors suitable for specific tasks. In the regions of magnetic chicanes i.e. the bunch compressors and collimator (figure 1), the probability of collision of the transversally diffused component of the primary accelerated electrons with the beam tube is very high, resulting in the production of intense radiation field including a large number of prompt secondary photo neutrons. Undoubtedly, the most intense flux of neutrons is produced in the water-cooled copper beam dump situated in an underground chamber made of 2 m thick concrete blocks (figure 1).

After the final stage of acceleration (post-accelerator module #5) the 1 GeV electron beam is collimated by the 50 m long collimator and then injected into the undulators. The radiation measurements were carried out at selected locations (figure 1) representing the typical installation sites of the electronic instrumentation vital to accelerator control systems of the FLASH [2] as well as the future XFEL currently under construction in Hamburg [9]. The scope of neutron and gamma dosimetry emphasizing the type of dosimeters used is summarized as follows.

- For the assessment of fast neutrons generated at highly localized spots as described above, we have attached five commercial off-the-shelf (COTS) GaAs LEDs [4], packed in tiny satchels made of thin plastic material, at the locations p1, p2, p3, p4 and p5 (figure 1).
- At location N (figure 1), 113 m from the reference point (RF gun) and 3 m from the accelerator module #5 the neutron spectrum was evaluated using four (a, b, c, d) temperature compensated superheated emulsion (bubble) detectors [5].
- At location W (figure 1), 148 m from the reference point (RF gun) and 1.2 m from the beam tube the bremsstrahlung gamma spectrum was assessed using a simple gamma spectrometer based on TLD-700 dosimeter chips enclosed in a wedge shape attenuator made of lead [6].

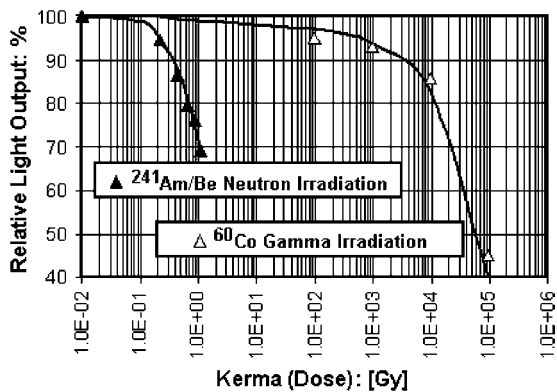


**Figure 3.** Showing the relative light output of GaAs LEDs irradiated with neutrons and photons from standard sources. The light outputs are normalized with the control (unirradiated) LEDs.

(d) On the surface of the accelerator modules (figure 1), we have estimated *in situ* the gamma and neutron doses using radiochromic (Gaf-EBT) film dosimeters [7] and bubble detectors [5], respectively. We also have investigated the effects of voltage gradients across the cavities belonging to accelerator modules 4 and 5 in the production of field emission induced radiation fields [12].

## 2.2. Estimation of neutron fluence rate using GaAs LEDs

The non-ionizing energy loss (NIEL) of fast neutrons in unbiased GaAs light emitting diodes (LEDs) results in the reduction of the light output [14]. The exposure to photons on the other hand reveals they have much less effect on the reduction of light emission. We have irradiated batches of commercially available miniature (3 mm diameter) yellow GaAs LEDs (model: LN48YPX, Manufacturer: Panasonic Corporation, Japan) with gamma rays from a  $^{60}\text{Co}$  source up to  $9.8 \times 10^4$  Gy and with neutrons from an  $^{241}\text{Am/Be}$  ( $\alpha, n$ ) source up to 1.9 Gy (GaAs kerma). The light output of the irradiated and control (unirradiated) LEDs was evaluated using a simple microprocessor based photometer developed at our laboratory [4, 15]. In figure 3, the light output of neutron and photon irradiated LEDs is depicted as a function of kerma.

The kerma in GaAs and the resulting light output are strongly related to the neutron energy distribution (spectrum). The batches of LED used in this investigation were first calibrated with neutrons from an  $^{241}\text{Am/Be}$  source (average energy: 4.3 MeV). However, for real-life application of the GaAs LEDs as neutron dosimeters in the FLASH environment, the initial calibration factor was modified for a giant dipole resonance (GDR) photoneutron spectrum (average energy  $\sim 2$  MeV) using the corresponding fluence to kerma conversion factors (unit:  $\text{Gy cm}^2$ ) and energy distributions. The calibration procedure of the GaAs LEDs has been discussed in detail elsewhere [4]. The neutron fluence is plotted as a logarithmic function of relative light output and presented in figure 4. Evidently, this plot serves as the calibration curve of the GaAs LED based neutron fluence monitor for FLASH producing neutrons with a GDR energy distribution. The displacement damage (kerma) of neutrons in the GaAs LEDs is directly proportional to energy starting from 1 keV and increases

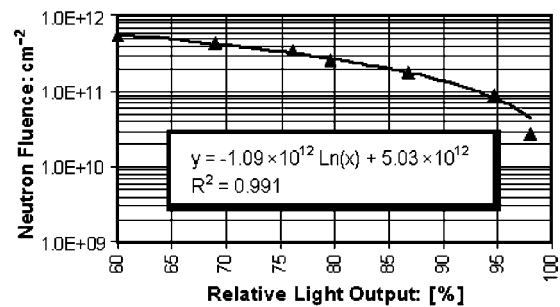


**Figure 4.** The neutron fluence (FLASH spectrum) is shown as a logarithmic function (inset) of the relative light output of the GaAs LEDs.

linearly up to an excess of 10 MeV [14]. Evidently, the response of the GaAs LEDs to low-energy (thermal) neutrons is predicted to be negligibly small, hence has been ignored in our work.

We have used the calibration curve of the GaAs LEDs (figure 4) to evaluate neutron fluence at five locations along the FLASH beam line (p1, p2, p3, p4 and p5) where a high probability of impact of energetic electrons with the internal wall of the beam tube is expected (figure 1). Batches of GaAs LEDs (with 5 LEDs per batch) were attached to selected spots along the FLASH beam line and exposed for six routine linac operation days. The LEDs were retrieved and assessed [15]; the results are shown in figure 5.

Unlike the well-known thermoluminescence dosimeters (TLD), the GaAs LEDs used in our investigations showed no evidence of long term (3 months) fading at ambient (room) temperature. However, experimental results from other investigators demonstrated a significant recovery (annealing) of displacement damage in GaAs LEDs when heated to 270 °C for 2 h [14].

In order to prove the highly localized nature of neutron emission, we have recorded the gamma dose rate along the beam pipe between points p1 and p2 (figure 1) using a gamma survey meter (model: 6150 AD-2; manufacturer: Autometrics, Germany) connected to a 2.5 cm diameter NaI(Tl) scintillation detector (model: 6150 AD-18). The gamma dose rates are plotted as a function of distance from the ‘hotspot’ (the region where the highest gamma radiation level was registered) and depicted in figure 6.

Evidently, the gamma dose results from the activation products in the beam pipe generated by neutron interaction. The rapid drop of gamma dose with the distance (figure 6) confirms the neutrons were produced locally, i.e. by the impact of accelerated electrons with the beam pipe. Therefore, the relative neutron fluence ( $N_x/N_0$ ) at a distance  $x$  cm from the central axis of the beam pipe could be predicted by the inverse square law:

$$\frac{N_x}{N_0} = \left(\frac{r}{x}\right)^2 \quad (2)$$

where  $N_x$  and  $N_0$  are the neutron fluences at a distance of  $x$  (cm) from the central axis of beam pipe and at the surface of the beam pipe, i.e. location of LEDs respectively;  $r = 2.5$  cm, the radius of the beam pipe. Hence, the relative neutron fluence at 1 m from the beam tube ( $x = 100$  cm) was calculated to be  $6.25 \times 10^{-4}$  (equation (2)).

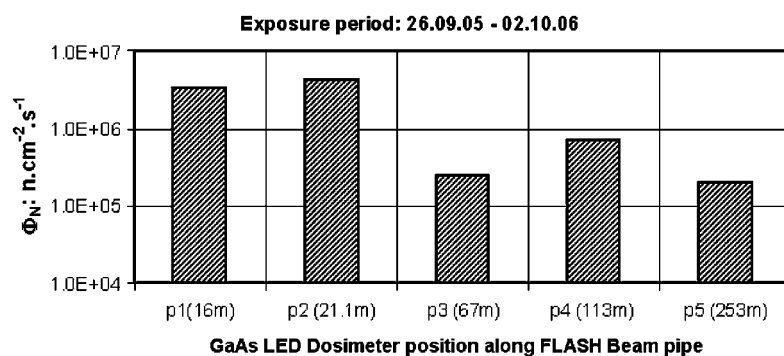


Figure 5. Neutron fluence rates at several critical locations along the FLASH beam pipe evaluated using GaAs LED dosimeters.

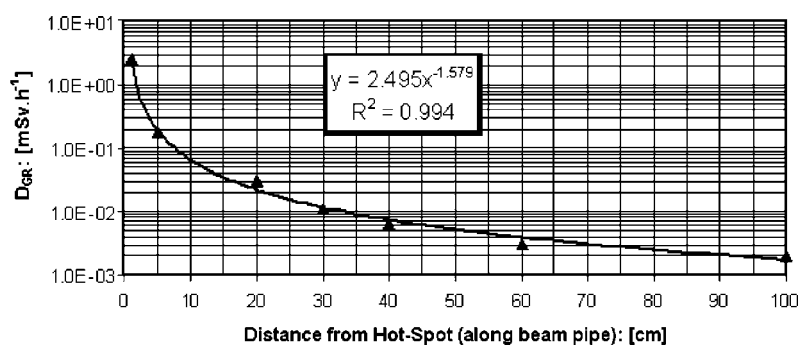


Figure 6. Showing the drop of gamma dose rate ( $D_{GR}$ ) from the ‘hot spot’ as a function (shown inset) of distance, measured laterally along the beam pipe.

### 2.3. Estimation of neutron energy spectrum using bubble detectors

A copious number of photoneutrons are produced due to the interaction of high-energy bremsstrahlung photons with the material of the FLASH beam pipe. The electron linac driving the FLASH operates in pulsed (5–10 Hz) mode, hence, conventional neutron monitors (rem counters) prone to pulse dead time effect are inappropriate for the detection of such a neutron field [3]. The superheated emulsion (bubble) dosimeters are integrating devices, making them ideal for pulsed neutron detection. We have used two types of temperature compensated detectors: (a) BDPND (neutron sensitivity range: 100 keV–15 MeV) and (b) BDT (effective energy response at 0.025 eV, i.e. thermal) to estimate the neutron fluence [16]. The neutron sensitivity factor (unit:  $\mu\text{Sv}/\text{bubble}$ ) of BDPND type detectors remains constant (flat) within the energy band ‘100 keV–15 MeV’. This means, for neutrons with energy below 100 keV, the bubble detectors show negligible response and at energy above 15 MeV the detector response falls sharply [5]. We have extended the energy response of BDPND type bubble detectors to 130 MeV by enclosing them in a lead capsule of 2 cm wall thickness [17].

Pairs of BDPND (both of sensitivity 14.5  $\mu\text{Sv}/\text{bubble}$ ) and BDT (both of sensitivity 0.385  $\mu\text{Sv}/\text{bubble}$ ) type bubble detectors were assembled in the following manner: (a) BDPND #1/in a lead capsule, (b) BDPND #2/bare, (c) BDT #1/in a cadmium capsule of 2 mm wall thickness and (d) BDT #2/bare. The dosimeter assembly was mounted on the FLASH tunnel wall, 3 m from the far end of accelerator

module 5 (figure 1). After a routine exposure period of 7 days (19.09.06 to 26.09.06) the dosimeters were retrieved, and digitally photographed (four pictures for each detector 90° apart). The digital pictures were evaluated by using an optical bubble counting algorithm (OBCA) developed at our laboratory [18].

The method of neutron fluence evaluation from the number of bubbles counted in all four detectors (a, b, c, d) is presented as follows.

*Bin 1 (thermal neutron).* The neutron equivalent dose ( $H_1$ ) was calculated as

$$H_1 = s1[\text{Nav}(\text{BDTc}) - \text{Nav}(\text{BDTd})] \quad (3a)$$

where  $\text{Nav}(\text{BDTc})$ ,  $\text{Nav}(\text{BDTd})$  and  $s1$  are the average number of bubbles counted in bare and cadmium-shielded detectors and the dosimeter sensitivity factor, respectively.

The thermal neutron fluence was calculated as

$$\Phi_1 = H_1/F_1 \quad (3b)$$

where  $F_1$  ( $5.4 \times 10^{-6} \mu\text{Sv cm}^2$ ) is the fluence to effective dose equivalent conversion coefficient for thermal neutrons [19].

*Bin 2 (neutrons within 0.1–15 MeV energy band).* The equivalent dose  $H_2$  and fluence  $\Phi_2$  were calculated as

$$H_2 = s2\text{Nav}(\text{BDPNDb}) \quad (4a)$$

$$\Phi_2 = H_2/F_2 \quad (4b)$$

where  $\text{Nav}(\text{BDPNDb})$ ,  $F_2$  ( $4.07 \times 10^{-4} \mu\text{Sv cm}^2$ ) and  $s2$  are the average number of bubbles counted in the bare BDPND type detector, the fluence to effective dose equivalent

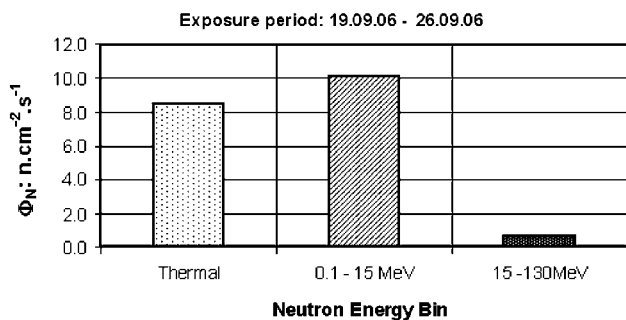


**Figure 7.** The three-bin neutron spectrum near accelerator module #5 of the FLASH evaluated using superheated emulsion (bubble) detectors.

conversion coefficient [19] and detector sensitivity factor, respectively.

*Bin 3 (neutrons within 15–130 MeV energy band).* The equivalent dose  $H_3$  and fluence  $\Phi_3$  within the 15–130 MeV energy band (augmented neutron energy range) are given as

$$H_3 = s2[\text{Nav}(\text{BDPNDa}) - \text{Nav}(\text{BDPNDb})] \quad (5a)$$

$$\Phi_3 = H_3/F_3 \quad (5b)$$

where  $\text{Nav}(\text{BDPNDa})$ ,  $\text{Nav}(\text{BDPNDb})$  and  $F_3$  ( $5.62 \times 10^{-4} \mu\text{Sv cm}^2$ ) are the average number of bubbles counted in lead encapsulated and bare BDPND type detectors and the fluence to effective dose equivalent conversion coefficient [19], respectively.

The three-bin neutron energy spectrum evaluated using a set of bubble detectors at the high-energy end of the linac is shown in figure 7.

The sensitivity factors  $s1$  (BDPND type detector) and  $s2$  (BDT type detector) were originally evaluated by the manufacturer (BTI Industries, Ont., Canada) using an  $^{241}\text{Am}/\text{Be}$  neutron calibration source [5] and included in the quality assured (QA) calibration certificate supplied with those detectors. We have re-evaluated the above sensitivity factors using a similar  $^{241}\text{Am}/\text{Be}$  neutron source (source strength:  $2.12 \times 10^6$  neutrons  $s^{-1}$ ), the results agreed within an uncertainty level of  $\pm 10\%$ . Furthermore, the fluence to effective dose equivalent conversion coefficient (0.1–15 MeV band) was also calculated and found to be  $3.42 \times 10^{-4} \mu\text{Sv cm}^2$ , compared to  $4.07 \times 10^{-4} \mu\text{Sv cm}^2$  derived from [19]. The method of thermal neutron dosimetry using BDT type bubble detectors has been discussed in detail elsewhere [16].

The main goal of this work was the derivation of the neutron fluence in the FLASH environment from the number of bubble counts and the associated fluence to effective dose equivalent conversion coefficient. The sensitivity factors of the bubble detectors under calibration conditions ( $^{241}\text{Am}/\text{Be}$  neutrons) were valid for the experimental conditions at FLASH for the following reasons.

- A close similarity between the FLASH (giant dipole resonance) and the  $^{241}\text{Am}/\text{Be}$  neutron spectra [20] and
- constant sensitivity, i.e. ‘flat response’, of the bubble detectors within the neutron energy band (0.1–15 MeV) of interest [5]. Evidently, the neutron fluence at FLASH has

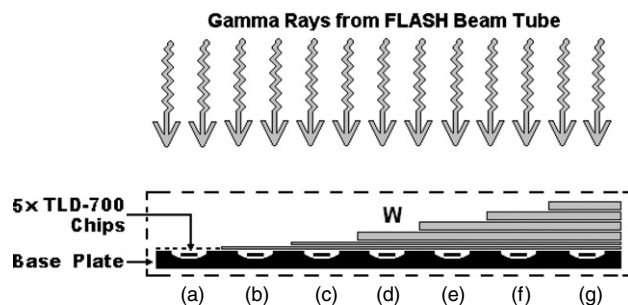


**Figure 8.** Showing the construction details of the lead attenuator wedge used for the unfolding of a bremsstrahlung spectrum at FLASH.

been parametrized using the fluence from an  $^{241}\text{Am}/\text{Be}$  calibration source. Hence, application of the operational quantities like dose weighting factor ( $W_R$ ) or quality factor (QF) recommended by ICRP/ICRU in neutron fluence calculation became irrelevant [19].

#### 2.4. Estimation of a bremsstrahlung spectrum using thermoluminescent dosimeters

Bremsstrahlung is the major source of radiation exposure in the electron linac tunnel [21] causing damage to electronic components due to the total ionising dose (TID) effect, manifested by the gradual degradation of the operational characteristics of the electronic components [22]. We have estimated the bremsstrahlung fluence spectrum in the FLASH tunnel using batches of TLD-700 ( $^7\text{LiF}:\text{Ti, Mg}$ ) chips enclosed in a 20 cm long wedge-shaped lead attenuator of the following step thicknesses: (a) 0 mm (none), (b) 1 mm, (c) 2 mm, (d) 7 mm, (e) 12 mm, (f) 17 mm and (g) 22 mm (figure 8). Forty commercially available TLD-700 chips (dimension:  $3.2 \times 3.2 \times 0.9 \text{ mm}^3$ ) were annealed and divided into eight batches each comprising five chips. The TLD chips from the first to seventh batches were placed under steps (a)–(g) (figure 8), whereas the eighth batch was stored in a safe place as a control. The lead wedge was placed at ground level, 1.5 m from the beam tube and 148 m from the RF gun, i.e. the reference point (figure 1). The lead-attenuator assembly housing the TLD chips was exposed to bremsstrahlung photons for one routine 6 day linac operation period.

The TLD chips were retrieved and evaluated at a ramp-heating rate of  $10^\circ\text{C s}^{-1}$ . The TL-output of the eighth batch (background/control) was subtracted from the readings of the other seven batches to obtain the net TLD-output [6]. The TLD-outputs, proportional to bremsstrahlung photon dose, were normalized with the output of the unattenuated batch (a). The data were analysed using the inverse calculation method based on a genetic algorithm [23] to unfold the bremsstrahlung spectrum as shown in figure 9. The result was compared with the computer-simulated spectrum [24]. The bremsstrahlung unfolding method using a lead wedge has been described in detail elsewhere [6].

#### 2.5. Application of radiochromic films as gamma dosimeter

Radiochromic films are thin, transparent foils made of plastic material with a coating of a novel radiosensitive material.

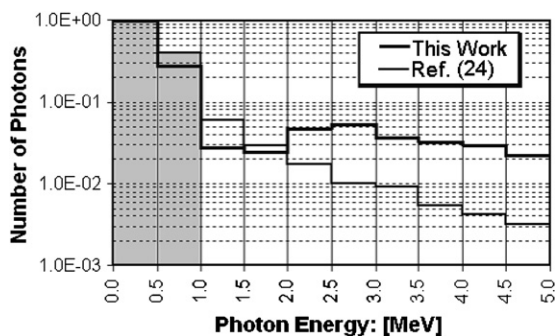


**Figure 9.** Showing the unfolded bremsstrahlung spectrum at FLASH and the computer-simulated spectrum adopted from reference.

Radiation exposure, in particular with gamma rays, creates colouration in the film. The radiochromic films are auto developing and the resulting optical density is proportional to absorbed dose. A new type of radiochromic film under the trade name Gafchromic EBT (Gaf-EBT) film, manufactured by the ISP (International Speciality Products, NJ, USA) is now available on the market. The Gaf-EBT film possesses a large dynamic dosimetry range (0.01–8.0 Gy), high response to high-energy gamma rays ( $^{60}\text{Co}$ ) but insensitive to neutrons. These unique properties make the Gaf-EBT film the most suitable candidate for a cost effective gamma dosimeter in a particle accelerator environment. Henceforth, we are extensively using these films for all major dosimetry related tasks at FLASH. Important physical and dosimetric characteristics of Gaf-EBT film have been extensively discussed elsewhere [7].

**2.5.1. Calibration of Gaf-EBT gamma dosimeter.** Six pieces of Gaf-EBT film (dimension  $1.5 \times 1.0 \text{ cm}^2$ ) were cut from the standard  $25 \times 20 \text{ cm}^2$  sheet, five segments were irradiated with a  $^{60}\text{Co}$  gamma source to 0.21, 0.49, 1.12, 2.10 and 3.01 Gy and the sixth kept as control. The films have a high spectral absorbance at 676 nm [25]; hence, we have used commercially available red LED ( $\lambda = 626 \text{ nm}$ ) to estimate the optical density (OD) of the irradiated films. The optical density is defined as

$$\text{OD} = -\log_{10}(I/I_0) \quad (6)$$

where  $I$  and  $I_0$  are the intensity of the light ( $\lambda = 626 \text{ nm}$ ) transmitted through the irradiated and control dosimeter films, respectively. We have used a sensitive digital photometer developed at our laboratory for light measurement [26]. The results are depicted in figure 10.

## 2.6. Radiation dosimetry at accelerator modules operating in field emission mode

The phenomenon of a field emission/dark current induced radiation field has been discussed in section 1.2 of this paper. During the field emission mode of operation, the RF gun of the linac is switched off, the accelerator module(s) under investigation are isolated from the neighbouring modules but the usual RF field across the cavities remains uninterrupted.

We have estimated the effective dose equivalent rate of neutrons ( $H_N$ ) and gamma dose rate ( $D_G$ ) at the outer surface

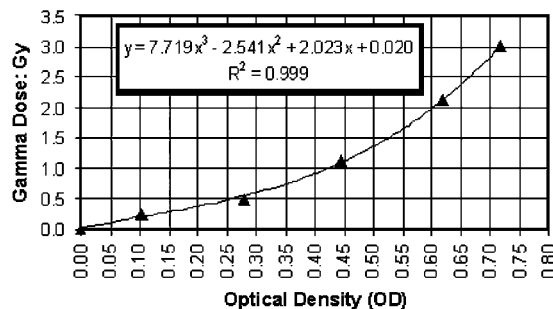


**Figure 10.** Showing the gamma dose delivered to the Gaf-EBT film as a function of optical density. The data points are fitted with the calibration polynomial (inset).

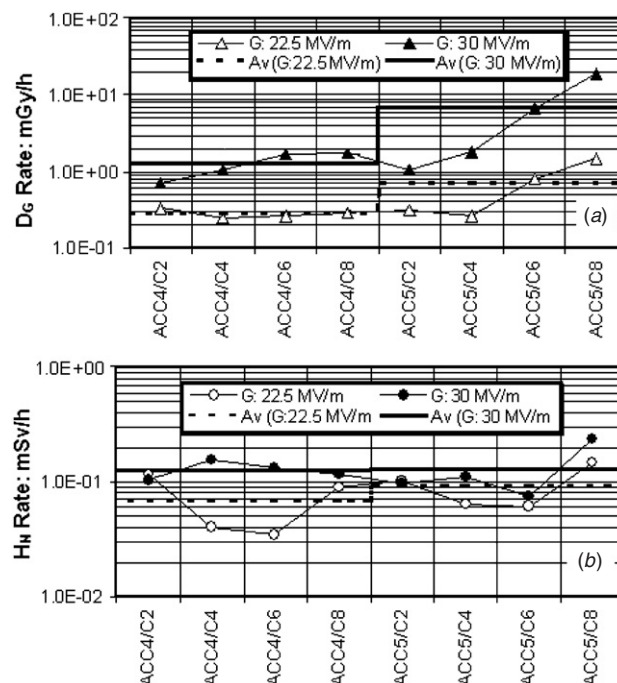


**Figure 11.** Showing (a) gamma dose rate  $D_G$  and (b) effective dose equivalent rate of neutrons  $H_N$  near accelerator modules #4 and #5 evaluated using Gaf-EBT films and bubble detectors respectively. The gradient across the modules and the average neutron and gamma dose rates are also indicated.

of accelerator modules 4 and 5 using calibrated superheated emulsion (bubble) detectors and Gaf-EBT film dosimeters respectively. Pairs of Gaf-EBT films and bubble detectors were placed at the top the accelerator module, opposite to every second cavity of accelerator modules #4 and #5 (position  $P_Z$  shown in figure 2). The radiation doses were assessed at two accelerator operating conditions: (a) gradient across the modules #4 and #5 set at  $22 \text{ MV m}^{-1}$ , exposure duration 17 h 30 min, (b) gradient across the modules #4 and #5 set at  $30 \text{ MV m}^{-1}$ , exposure duration 26 h 10 min. The duty cycle (pulse repetition rate) was set at 10 Hz for both cases. The results are presented in figure 11.

## 2.7. Radiation dosimetry at accelerator modules operating in routine mode

During routine mode operation (5 Hz repetition rate) of the FLASH, the RF gun remains switched on, the electron beam

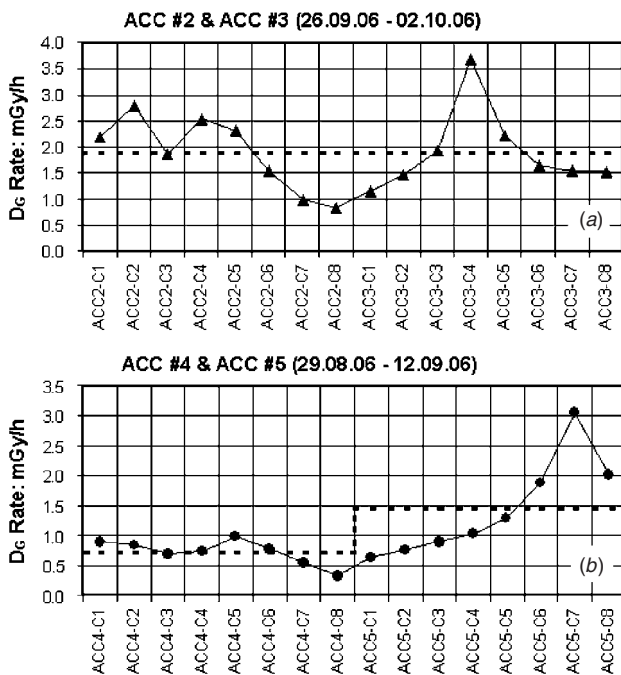


**Figure 12.** Showing the gamma dose rates  $D_G$  near the accelerator module pairs #2 and #3 (a) and #4 and #5 (b) evaluated using Gaf-EBT films during routine operation mode. The average gamma dose rates are indicated by the dotted lines. Modules #2, #3 and #5 were operating at the gradient of  $21 \text{ MV m}^{-1}$  whereas the module #4 operated at  $16 \text{ MV m}^{-1}$ .

is accelerated via all five accelerator modules and ultimately stopped in the underground beam dump (figure 1). In this case, we have estimated only the gamma doses while all five modules were operating at a gradient of  $21 \text{ MV m}^{-1}$ . Eight Gaf-EBT gamma dosimeter foils were placed opposite to each cavity of the modules #2, #3, #4 and #5 along the equator (position  $P_E$  shown in figure 2). After routine exposure the Gaf-EBT films were evaluated [26] and the results are shown in figure 12.

### 3. Data analysis and interpretation

In the framework of the present research project at DESY, we have evaluated the neutron and gamma dose, fluence and spectra at various selected locations in the FLASH tunnel using an assortment of novel passive dosimeters.

- (a) The neutron fluence rates in the close proximity of the bunch compressors and collimator (at direct contact) were estimated with tiny GaAs LEDs. The neutron fluence at several highly localized spots was measured to be  $>10^6 \text{ cm}^{-2} \text{ s}^{-1}$  (figure 5). Evidently, the high neutron fluence emanating from a localized point source drops to a factor  $6.25 \times 10^{-4}$  at a lateral distance of 1 m from the beam pipe (equation (2)), hence causes little concern to the radiation health of microelectronic devices in the vicinity. The effects of room-scattered neutrons were ignored due to negligibly low sensitivity of GaAs to slow neutrons [4, 14, 27] and the extremely short distance between the detector (LED) and the neutron source, the ‘hotspot’ at the beam pipe.

- (b) A simple three-bin neutron spectrum was evaluated using BDPND (fast neutrons) and BDT (thermal neutrons) type superheated emulsion (bubble) detectors at 3 m from the accelerator module #5. The result (figure 7) confirms the predominance of GDR neutrons with a peak energy within 13–18 MeV in the FLASH tunnel, in agreement with the data given in [20, 21]. The presence of a significant number of wall-scattered slow (thermal) neutrons has also been indicated (figure 7).
- (c) The bremsstrahlung gamma spectrum at  $90^\circ$  (lateral) with the beam propagation direction was estimated using batches of TLD-700 chips enclosed in a stepped wedge shape lead attenuator. The peak and average photon energy were evaluated to be 500 and 800 keV respectively. Our results agreed well with the computer-simulated spectrum presented elsewhere [24]. Above the gamma energy level of 5 MeV, the half value layer (HVL) thickness of lead begins to drop (instead of rising), thereby setting the highest limit of an unfolded bremsstrahlung spectrum at 5 MeV. This limitation, however, has no influence in the scope of this work, as more than 90% of the photons within the bremsstrahlung spectrum are contained within the energy band 0–1 MeV [6, 24].
- (d) The field emission/dark current induced gamma doses and neutron effective dose equivalents at the surface of the accelerator modules 4 and 5 were evaluated at the gradients  $22.5$  and  $30 \text{ MV m}^{-1}$  (figure 11). The BDPND type bubble detectors and Gaf-EBT film dosimeters were used for the assessment of neutron and gamma doses, respectively. The peak gamma dose rates (cavity 8 of module 5) operating at gradients  $22.5$  and  $30 \text{ MV m}^{-1}$  were estimated to be  $1.5$  and  $19 \text{ mGy h}^{-1}$  respectively. The corresponding neutron effective dose equivalents were, on the other hand,  $0.12$  and  $0.25 \text{ mSv h}^{-1}$  at the gradients  $22.5 \text{ MV m}^{-1}$  and  $30 \text{ MV m}^{-1}$ , respectively. The sharp jump of gamma dose rate with increased gradient is elucidated with the Fowler Nordheim field emission theory [11, 12]. The gamma dose rate ( $19 \text{ mGy h}^{-1}$ ) at a gradient of  $30 \text{ MV m}^{-1}$  found to be 76 times higher than the corresponding neutron dose equivalent rate ( $0.25 \text{ mSv h}^{-1}$ ). This is explained as follows: the secondary gamma radiation is produced by the interaction of the intense electric charge (field emission) of lower energy with the cavity wall. On the other hand, the neutrons are produced by much less intense (diluted) electric charge, however, accelerated to a much higher energy in order to overcome the nuclear reaction threshold for neutron production [28].
- (e) The gamma dose rates at accelerator modules #2, #3, #4 and #5 during routine operation mode were estimated using Gaf-EBT films (figure 12). All modules except #4 were running at the gradient of  $21 \text{ MV m}^{-1}$ . The average gamma dose rate at modules #2 and #3 was  $1.8 \text{ mGy h}^{-1}$ , whereas the average gamma doses at modules #4 (gradient:  $16 \text{ MV/m}$ ) and #5 (gradient:  $21 \text{ MV/m}$ ) were evaluated to be  $0.71$  and  $1.48 \text{ mGy h}^{-1}$  respectively.

### 4. Summaries and conclusion

We have estimated the effective neutron dose equivalents and gamma doses as well as energy distributions (spectra)

**Table 2.** Results of the radiation measurements carried out in the FLASH tunnel under various linac operation conditions. The repetition rates for *routine* and *field emission* operation modes were set at 5 Hz and 10 Hz, respectively.

Location	Radiation type	Quantity (unit)	Value	Remarks
Beam line	Fast neutron: (figure 5) <i>routine mode</i>	Fluence rate: (neutron cm <sup>-2</sup> s <sup>-1</sup> )	4.4 × 10 <sup>6</sup> (max) at p2 2.0 × 10 <sup>5</sup> (min) at p5	Using GaAs LEDs, neutron fluence drops by a factor of (6.25 × 10 <sup>-4</sup> ) at 1 m
113 m from RF gun, 3 m from accelerator mod. 5	Photo neutron spectrum: (figure 7) <i>routine mode</i>	Fluence rate: (neutron cm <sup>-2</sup> s <sup>-1</sup> )	(a) 8.4 × 10 <sup>0</sup> (b) 1.01 × 10 <sup>1</sup> (c) 7.1 × 10 <sup>-1</sup>	(a) Thermal (b) 0.1–15 MeV (c) 15–130 MeV Using BDPND and BDT type detectors
148 m from RF gun	Bremsstrahlung spectrum: (figure 9) <i>routine mode</i>	Fluence (relative)	(a) 1.0 (0.5 MeV) (b) 0.3 (1 MeV) (c) 0.02 (>1 MeV)	Using TLD-700 chips and a multi-stepped wedge made of ordinary lead
Accelerator modules 4 and 5	Gamma rays: <i>field emission mode</i>	Dose rate: (mGy h <sup>-1</sup> )	(a) 19.0 (max) (b) 1.5 (max)	(a) G = 30.0 MV m <sup>-1</sup> (b) G = 22.5 MV m <sup>-1</sup>
Accelerator modules 4 and 5	Fast neutrons: <i>field emission mode</i>	Dose equivalent rate: (mSv h <sup>-1</sup> )	(a) 2.36 × 10 <sup>-1</sup> (max) (b) 1.48 × 10 <sup>-1</sup> (max)	(a) G = 30.0 MV m <sup>-1</sup> (b) G = 22.5 MV m <sup>-1</sup>
		Fluence rate: (neutron cm <sup>-2</sup> s <sup>-1</sup> )	(a) 1.92 × 10 <sup>2</sup> (max) (b) 1.21 × 10 <sup>2</sup> (max)	(a) G = 30.0 MV m <sup>-1</sup> (b) G = 22.5 MV m <sup>-1</sup>
Accelerator modules 2 and 3	Gamma rays: <i>routine mode</i>	Dose rate: (mGy h <sup>-1</sup> )	(a) 3.7 (max) (b) 1.98 (average)	(a) G = 21 MV m <sup>-1</sup> (b) G = 21 MV m <sup>-1</sup>
Accelerator module 4	Gamma rays: <i>routine mode</i>	Dose rate: (mGy h <sup>-1</sup> )	(a) 1.0 (max) (b) 0.71 (average)	(a) G = 16 MV m <sup>-1</sup> (b) G = 16 MV m <sup>-1</sup>
Accelerator module 5	Gamma rays: <i>routine mode</i>	Dose rate: (mGy h <sup>-1</sup> )	(a) 3.2 (max) (b) 1.48 (average)	(a) G = 21 MV m <sup>-1</sup> (b) G = 21 MV m <sup>-1</sup>

at various important locations in the FLASH tunnel. The measurements were carried out for routine operation as well as for field emission (dark current) mode of the linac. The results are summarized in table 2.

Using a combination of various passive dosimeters we have analysed the important characteristics of the radiation fields prevailing in the FLASH tunnel. The field emission/dark current was found to be the most significant source of radiation in the FLASH environment. The levels of both neutron and gamma doses and fluence rates associated strongly with the gradients across the accelerator modules. The gamma dose rate was found to be about 80 times higher than the effective neutron dose equivalent rate. The fluence of photo-neutrons of energy 0.1 to 15 MeV, generated via the GDR reaction, was evaluated to be more than one order of magnitude higher than that of neutrons with energy higher than 15 MeV. A significant level of thermal neutrons, produced by the scattering of primary (fast) neutrons with the concrete wall of the tunnel, was also recorded.

Localized (i.e. confined in small spots) regions producing high neutron yield (fluence) were measured near the bunch compressors and collimator using GaAs LED. However, this fluence drops rapidly with distance following the inverse square law, hence, poses little radiological impact to objects located in the proximity.

The results of the present radiation measurement investigations will provide important guidelines relevant to various essential radiological safety and radiation effects related aspects of the FLASH as well as the future XFEL facility in Hamburg [29]. Some points worth mentioning are as follows: (a) radiation sensitive devices should not

be mounted in the vicinity of the bunch compressors or collimators producing intense localized neutron radiation, (b) by considering the worst case scenario, i.e., accelerator module #5 running a gradient of 30 MV m<sup>-1</sup> (table 2), the integrated gamma dose in 10 years of operation time was calculated as 1.66 kGy. Similarly, the integrated neutron fluence at accelerator module #5 was calculated as 6.06 × 10<sup>10</sup> neutron cm<sup>-2</sup>. Using the fluence-to-kerma conversion factor of silicon [22, 27], the accumulated neutron kerma in 10 years in silicon (major building material of microelectronics) was calculated as 50 mGy. (c) Gamma dose (kerma) is more than four orders of magnitude higher than neutron kerma (Si). (d) Using the experimental data (average values) in table 2, we have calculated the yearly quota (routine operation) of gamma dose (kerma), neutron fluence and neutron kerma (Si) as 12 Gy/a, 3.80 × 10<sup>9</sup> neutron cm<sup>-2</sup>/a and 3.0 mGy/a respectively. (e) The presence of a significant number of low energy (thermal) neutrons in the FLASH tunnel, predominantly produced by room/wall scattering effect (table 2), may cause single event upset (SEU) in microelectronic memories [22]. The simplest choice for the mitigation of SEU is to cover the microelectronic device with boron-based shielding material of appropriate thickness. (f) An unfolded bremsstrahlung spectrum (figure 9) could be useful for the estimation of optimal lead shield thickness for the reduction of gamma dose. (g) Evidently, the gamma radiation constitutes the primary source of total ionizing dose (TID) effect, detrimental to the radiation health of microelectronic devices operating in the FLASH environment. (h) At high-energy accelerators, the threshold of displacement damage lies at the neutron

fluence of  $10^{10} \text{ cm}^{-2}$  [30]. Hence, neutrons will play an insignificant role to cause long-term, irreversible damage to microelectronic devices located in the FLASH tunnel. Therefore, surveillance of the gamma radiation field in real-time, as well as in passive mode, is imperative to safe and reliable operation of the electron linac driving the FLASH.

## References

- [1] Brinkmann R, Flottmann K, Rossbach J, Schmuser P, Walker N and Weise H 2001 *TESLA Technical Design Report: Part II. The Accelerator* Deutsches Elektronen-Synchrotron DESY
- [2] Simrock S 2004 State of the art RF control *Linac 2004 Proc.* pp MO102/8-/11
- [3] Liu J C, Rokni S, Vylet V, Arora R, Semones E and Justus A 1997 Neutron detection time distributions of multisphere LiI detectors and AB rem meter at a 20 MeV electron linac *Radiat. Prot. Dosim.* **71** 251–9
- [4] Mukherjee B, Rybka D, Simrock S, Khachan J and Romaniuk R 2006 Application of low cost gallium arsenide light emitting diodes as kerma dosimeter and fluence monitor for high-energy neutrons *Radiat. Prot. Dosim.* at press
- [5] Ing H, Noulty R A and McLean T D 1997 Bubble detectors—a maturing technology *Radiat. Meas.* **27** 573–7
- [6] Mukherjee B, Makowski D and Simrock S 2005 Dosimetry of high energy electron linac produced photoneutrons and bremsstrahlung gamma rays using TLD-500 and TLD-700 dosimeter pairs *Nucl. Instrum. Methods Phys. Res. A* **545** 830–41
- [7] Soares C G 2006 New developments in radiochromic film dosimetry *Radiat. Prot. Dosim.* **120** 100–06
- [8] Schreiber S 1999 First experiments with the RF gun based injector for the TESLA Test Facility linac *Particle Accelerator Conf. 1999 Proc.* pp 84–6
- [9] Brinkmann R 2004 Accelerator layout of the XFEL *Linac 2004 Proc.* pp 2–5
- [10] Limberg T, Molodozhentsev A, Petrov V and Weise H 1996 The bunch compression system at the TESLA Test Facility FEL *Nucl. Instrum. Methods Phys. Res. A* **375** 322–4
- [11] Gopych M, Gräf H D, Laier U, Müller W F O, Platz M, Richter A, Setzer S, Stascheck A, Watzlawik S and Weiland T 2005 Study of dark current phenomena in a superconducting accelerating cavity at the S-DALINAC *Nucl. Instrum. Methods Phys. Res. A* **539** 490–8
- [12] Graber J, Kirchgessner J, Moffat D, Knobloch J, Padamsee H and Rubin D 1994 Microscopic investigation of high gradient superconducting cavities after reduction of field emission *Nucl. Instrum. Methods Phys. Res. A* **350** 582–94
- [13] Brinkmann R, Materlik G, Rossbach J and Wagner A 1997 Conceptual design of a 500 GeV  $e^+e^-$  linear collider with integrated x-ray laser facility *ECFA 1997-182* Deutsches Elektronen Synchrotron (DESY), vol 1, pp 298–305
- [14] Griffin P J, Kelly J G, Leura T F, Barry A L and Lazo M S 1991 Neutron damage equivalence in GaAs *IEEE Trans. Nucl. Sci.* **38** 1216–24
- [15] Rybka D 2005 Integrated measurement systems for electronic devices operating in radiation environment *TESLA Report 2005-17* Deutsches Elektronen-Synchrotron
- [16] Vanhavere F, Loos M, Plompen A J M, Wattercamps E and Thierens H A 1998 Combined use of the BD-PND and BDT bubble detectors in neutron dosimetry *Radiat. Meas.* **29** 573–7
- [17] Sawamura T, Kaneko J H, Abe M, Tamura M, Murai I, Homma A, Fujita F and Tsuda S 2003 Effect of lead converter on superheated drop detector response to high-energy neutrons *Nucl. Instrum. Methods Phys. Res. A* **505** 29–32
- [18] Kalicki A 2005 The measurement station for research of effects of increased radiation on CCD and CMOS sensors (radiation effects on photonic devices) *TESLA Report 2005-18* Deutsches Elektronen-Synchrotron
- [19] Ferrari A, Pelliccioni M and Pillon M 1997 Fluence to effective dose equivalent conversion coefficients for neutrons up to 10 TeV *Radiat. Prot. Dosim.* **71** 165–73
- [20] Tesch K 1979 Data for simple estimate for shielding against neutrons at electron accelerators *Part. Acc.* **9** 201–6
- [21] Vylet V and Liu J C 2001 Radiation protection at high-energy electron accelerators *Radiat. Prot. Dosim.* **96** 333–43
- [22] Messenger G C and Ash M S 1992 *The Effects of Radiation on Electronic Systems* 2nd edn (Princeton, NJ: Van Nostrand Reinhold)
- [23] Mukherjee B and Simrock S 2006 Characterisation of the bremsstrahlung generated by a 450 MeV superconducting electron linac using the inverse calculation method based on a genetic algorithm *Radiat. Meas.* at press
- [24] Mao X S, Fasso A, Liu J C, Nelson W R and Rokni S 2000 90° Bremsstrahlung source term produced in thick targets by 50 MeV to 10 GeV electrons *SLAC-PUB* 7722
- [25] Butson M J, Chueng T and Yu P K N 2005 Absorption spectra variations of EBT radiochromic film from radiation exposure *Phys. Med. Biol.* **50** N135–N140
- [26] Lipka T 2006 A LABView based gamma detector using radiochromic films *BSc Diploma Thesis (Studienarbeit)* TU Hamburg-Harburg
- [27] Ougouuag A M, Williams J G, Danjaji M B, Yang S and Meason J L 1900 Differential displacement kerma cross sections for neutron interactions in Si and GaAs *IEEE Trans. Nucl. Sci.* **37** 2219–28
- [28] Silari M, Agosteo S, Gaborit J-C and Ulrichi L 1999 Radiation produced by the LEP superconducting RF cavities *Nucl. Instrum. Methods Phys. Res. A* **432** 1–13
- [29] [http://xfel.desy.de/xfelhomepage/index\\_eng.html](http://xfel.desy.de/xfelhomepage/index_eng.html)
- [30] Butterworth A, Ferrari A, Tsoulou E, Vlachoudis V and Wijnands T 2005 Estimate of radiation damage to low-level electronics of the RF-system in the LHC cavities arising from beam gas collisions *Radiat. Prot. Dosim.* **116** 521–4